

AgriLiRa4D: A Multi-Sensor UAV Dataset for Robust SLAM in Challenging Agricultural Fields

Journal Title
 XX(X):1–13
 ©The Author(s) 2016
 Reprints and permission:
 sagepub.co.uk/journalsPermissions.nav
 DOI: 10.1177/ToBeAssigned
 www.sagepub.com/

SAGE

Zhihao Zhan¹, Yuhang Ming², Shaobin Li¹, and Jie Yuan³

Abstract

Multi-sensor Simultaneous Localization and Mapping (SLAM) is essential for Unmanned Aerial Vehicles (UAVs) performing agricultural tasks such as spraying, surveying, and inspection. However, real-world, multi-modal agricultural UAV datasets that enable research on robust operation remain scarce. To address this gap, we present AgriLiRa4D, a multi-modal UAV dataset designed for challenging outdoor agricultural environments. AgriLiRa4D spans three representative farmland types—flat, hilly, and terraced—and includes both boundary and coverage operation modes, resulting in six flight sequence groups. The dataset provides high-accuracy ground-truth trajectories from a Fiber Optic Inertial Navigation System with Real-Time Kinematic capability (FINS-RTK), along with synchronized measurements from a 3D LiDAR, a 4D Radar, and an Inertial Measurement Unit (IMU), accompanied by complete intrinsic and extrinsic calibrations. Leveraging its comprehensive sensor suite and diverse real-world scenarios, AgriLiRa4D supports diverse SLAM and localization studies and enables rigorous robustness evaluation against low-texture crops, repetitive patterns, dynamic vegetation, and other challenges of real agricultural environments. To further demonstrate its utility, we benchmark four state-of-the-art multi-sensor SLAM algorithms across different sensor combinations, highlighting the difficulty of the proposed sequences and the necessity of multi-modal approaches for reliable UAV localization. By filling a critical gap in agricultural SLAM datasets, AgriLiRa4D provides a valuable benchmark for the research community and contributes to advancing autonomous navigation technologies for agricultural UAVs. The dataset can be downloaded from: <https://zhan994.github.io/AgriLiRa4D>.

Keywords

Dataset, Aerial Robots, Multi-Sensor Fusion, Agricultural Fields, Simultaneous Localization and Mapping, 4D Radar, LiDAR, Inertial Measurement Unit.

1 Introduction

The rapid advancement of agricultural technology has positioned Unmanned Aerial Vehicles (UAVs) as essential platforms for precision farming tasks such as crop monitoring, pesticide spraying, and large-scale farmland surveying (Radoglou-Grammatikis et al. (2020); Cheng et al. (2023); He et al. (2025); Wang et al. (2025b)). To operate safely and efficiently in these complex outdoor environments, agricultural UAVs require robust and accurate localization as a fundamental capability for autonomous navigation and task execution.

Although Global Navigation Satellite System (GNSS) positioning is widely used in agricultural applications, its performance often degrades severely due to vegetation occlusion, atmospheric disturbances, and multipath effects in structured farmlands (Pini et al. (2020)). As a result, GNSS alone is insufficient for reliable localization, particularly when UAVs operate near crop canopies or close to the terrain. These limitations motivate the adoption of Simultaneous Localization And Mapping (SLAM)-based approaches, which can provide continuous pose estimation when GNSS becomes unreliable.

However, conventional visual SLAM systems face their own challenges in agricultural environments. Dynamic illumination, repetitive and texture-sparse crop patterns, and low-light or low-temperature operating

conditions—commonly encountered during pesticide spraying—reduce the availability of stable visual features. In addition, high-speed UAV flight induces motion blur, while strong downwash airflow from heavy payloads causes vegetation motion, further destabilizing feature tracking and leading to frequent failures (Cadena et al. (2017); Mur-Artal and Tardós (2017)). These factors collectively limit the robustness of pure visual SLAM, underscoring the need for multi-sensor SLAM systems that integrate LiDAR, Radar, inertial sensing, and other modalities to achieve reliable localization in challenging agricultural settings.

Recent advances in multi-modal sensor fusion have demonstrated promising potential for enhancing SLAM robustness in challenging environments (Zuo et al. (2019);

¹TopXGun Robotics, Nanjing, 211100, China

²School of Computer Science, Hangzhou Dianzi University, Hangzhou, 310018, China

³School of Electronic Science and Engineering, Nanjing University, Nanjing, 210023, China

Corresponding author:

Yuhang Ming, School of Computer Science, Hangzhou Dianzi University, Hangzhou, 310018, China.

Jie Yuan, School of Electronic Science and Engineering, Nanjing University, Nanjing, 210023, China.

Email: yuhang.ming@hdu.edu.cn, yuanjie@nju.edu.cn

Shan et al. (2020b); Zheng et al. (2025). Light Detection and Ranging (LiDAR) sensors provide accurate and illumination-invariant geometric measurements, while emerging 4D Radar technology offers complementary advantages including weather robustness and direct velocity estimation Zhang et al. (2023); Zhuang et al. (2023). Fusing these ranging modalities with Inertial Measurement Units (IMUs) therefore offers a promising pathway to overcoming the inherent limitations of GNSS- and vision-based systems in agricultural UAV applications.

Despite the theoretical advantages of multi-modal sensing, the development and evaluation of robust agricultural UAV SLAM systems remain constrained by the lack of specialized datasets that comprehensively capture the operational diversity of agricultural missions. Existing datasets predominantly focus on urban or indoor scenarios Burri et al. (2016); Majdik et al. (2017); Nguyen et al. (2022), and only a few extending to semi-natural settings such as islands or rural towns Li et al. (2024). However, these semi-structured environments still differ substantially from real farmland, where unstructured terrain, heterogeneous vegetation, and large-scale outdoor operations introduce fundamentally different sensing and localization challenges. Agricultural UAVs must operate across a wide range of tasks, from low-altitude crop inspection to high-speed field mapping, each characterized by distinct motion dynamics and complex environmental interactions that critically affect SLAM robustness. These limitations highlight the need for a dedicated agricultural UAV dataset that systematically represents the sensing, motion, and environmental diversity inherent to real-world farming operations.

To address this critical gap, this paper introduces a novel multi-modal dataset specifically developed for agricultural UAV SLAM research, incorporating LiDAR, 4D Radar, and IMU measurements collected using an agricultural UAV platform. Our dataset features high-precision ground truth trajectories obtained from a Fiber Optic Inertial Navigation System (FINS) module with a built-in Real-Time Kinematic (RTK) receiver (hereafter denoted as FINS_RTK), ensuring centimeter-level position accuracy and high-fidelity orientation references. This work aims to advance the development of robust SLAM systems tailored for agricultural autonomous operations. Our contributions are summarized as follows:

1. **AgriLiRa4D Dataset:** We introduce a large-scale agricultural UAV dataset covering diverse terrain types, motion dynamics, and flight altitudes. The dataset provides synchronized LiDAR, 4D Radar, and IMU measurements, complemented by centimeter-level position and high-precision orientation ground truth from a FINS_RTK system.
2. **SLAM Benchmark:** We perform comprehensive evaluations of representative multi-sensor fusion SLAM algorithms (LiDAR-Inertial, Radar-Inertial, and Radar-LiDAR-Inertial) under varied agricultural conditions, providing quantitative insights into their localization accuracy, robustness, and adaptability to complex outdoor environments.

3. **Multi-Modal Fusion Analysis:** We analyze multi-sensor fusion strategies in challenging agricultural scenarios, highlighting how Radar-LiDAR-IMU integration enhances pose estimation consistency and robustness across different crop types, terrain slopes, and UAV flight regimes.

The remainder of this paper is organized as follows. Section 2 provides a detailed comparison between our dataset and existing benchmarks. Section 3 describes the UAV platform and sensing configuration used for data collection. Section 4 presents the characteristics of the dataset, highlighting the diverse agricultural scenarios and motion patterns. Section 5 reports experimental evaluations and analysis of three categories of state-of-the-art SLAM methods. Finally, Section 6 concludes the paper and outlines potential directions for future work.

2 Related Work

In this section, we review the existing multi-sensor UAV-included datasets and agricultural datasets, examining their sensor configurations, collection environments, ground-truth acquisition, and typical downstream tasks, to position our proposed dataset in the broader research landscape. All the reviewed datasets are listed in Table 1.

2.1 Multi-Sensor UAV-included Datasets

In recent years, multi-sensor fusion has become an increasingly popular paradigm for enhancing UAV autonomous navigation and localization. To address the challenges posed by complex and dynamic environments, modern pipelines have evolved from early visual-inertial frameworks to comprehensive multimodal configurations that integrate RGB, depth, stereo, LiDAR, event cameras, and GNSS/UWB signals. In line with this development, the research community has introduced a number of multi-sensor UAV datasets that serve as standard benchmarks for evaluating visual-inertial, LiDAR-visual, and other cross-modal navigation and localization systems. Depending on the operating environment, existing multi-sensor UAV datasets can be broadly divided into three categories.

Indoor or controllable environments. Representative datasets in this category include EuRoC Burri et al. (2016), UPenn Fast Flight Sun et al. (2018), and D^2 SLAM Xu et al. (2024). These datasets are collected in laboratories, offices, and warehouses under controlled motion profiles, stable lighting conditions, and limited environmental disturbances. They have become widely adopted benchmarks for evaluating highly dynamic SLAM and aggressive flight navigation.

Urban and campus environments. Examples include Zurich Urban MAV Majdik et al. (2017), NTU-VIRAL Nguyen et al. (2022), and GRACO Zhu et al. (2023). These datasets capture flights through structured building complexes, university campuses, and road networks, offering rich 3D geometry and frequently incorporating GNSS-based ground truth. They serve as key benchmarks for multimodal SLAM, collaborative perception, and GNSS-assisted navigation in structured human-made environments.

Table 1. Comparison of representative datasets grouped by platform type. Sensors are abridged; limitations summarize typical constraints reported in the original papers.

Platform	Dataset (Venue)	Sensors	Ground Truth	Environment	Primary Task	
Multi-Sensor UAV-included Datasets	Ariel	EuRoC (IJRR)	Stereo (gray); IMU	Laser; MoCap	Indoor lab	Visual-Inertial SLAM
	Ariel	Burri et al. (2016)				
	Ariel	Zurich Urban MAV (IJRR)	Mono (RGB); IMU	Photogrammetric reconstruction	Urban	SLAM; Reconstruction
	Ariel	Majdik et al. (2017)				
	Ariel	UPenn Fast Flight (RAL)	Stereo (gray); IMU	GPS	Warehouse; Woodland	Visual-Inertial SLAM
	Ariel	Sun et al. (2018)				
	Ariel	UZH-FPV (ICRA)	Event; Mono (RGB); Stereo (gray); IMU	Laser	Hanger; Grassland	Drone racing
	Ariel	Delmerico et al. (2019)				
	Ariel	NTU-VIRAL (IJRR)	Stereo (gray); LiDAR; IMU; UWB	Laser	Buildings	Multi-sensor SLAM
Ariel&Ground	GRACO (RAL)	Stereo (gray); LiDAR; IMU	INS; GPS	Campus	Collaborative SLAM	
Ariel	Zhu et al. (2023)					
Ariel	MARS-LVIG (IJRR)	Mono (RGB); LiDAR; IMU	RTK; DJI L1	Island; Town; Valley; Air-field	Multi-sensor SLAM	
Ariel	Li et al. (2024)					
Ariel	D ² SLAM (TRO)	Quad fisheye (RGB); RGB-D; IMU	MoCap	Office	Collaborative VI-SLAM	
Ariel	Xu et al. (2024)					
Ariel	FIREStereo (RAL)	Thermal stereo; LiDAR; IMU	SLAM algorithm	Woodland; Parking Lot	Depth; SLAM; Thermal perception	
Ariel	Dhrafani et al. (2025)					
Agricultural Datasets	Ground	Sugar Beets (IJRR)	Multi-spectral; RGB-D; LiDAR; GNSS	Manually labelled	Sugar-beet Fields	Classification; Mapping
	Ground	Chebroly et al. (2017)				
	Ground	Rosario (IJRR)	Stereo (RGB); IMU; Wheel Odom.	RTK	Soybean Fields	Multi-sensor SLAM
	Ground	Pire et al. (2019)		-	Orchard	Visual SLAM
	Ground	Macadamia Orchard (AuRo)	Stereo (RGB)			
	Ground	Islam et al. (2023)				
	Ground	CitrusFarm (ISVC)	Mono (gray); Stereo (RGB); Thermal; NIR; IMU; LiDAR	RTK	Orchard	Crop monitoring
	Ground	Teng et al. (2023)				
	Ground	Under-Canopy (IJRR)	Stereo (RGB); IMU; Wheel Odom.	RTK	Corn and Soybean Fields	Multi-sensor SLAM
	Ground	Cuaran et al. (2024)				
	Ground	GREENBOT (Sensors)	Stereo (RGB); LiDAR; IMU; GNSS	-	Greenhouse	SLAM
	Ground	Cañadas-Aránega et al. (2024)				
	Ground	MOLO-SLAM (Agriculture)	RGB-D; LiDAR; IMU	-	Grape and Tea Plantation	Semantic SLAM
	Ariel	Lv et al. (2024)				
	Ariel	GrapeSLAM (Data Br.)	Mono (RGB); IMU	RTK	Vineyard	SLAM; SfM
Ariel	Wang et al. (2025a)					
Ariel	WeedsGalore (WACV)	Multi-spectral	Manually labelled	Cotton Fields	Classification; Detection; Segmentation	
Ariel	Celikkan et al. (2025)					
Ariel	AgriLiRa4D	LiDAR; 4D Radar; IMU	FINS; RTK	Flat, Hilly, and Terraced Fields	Multi-sensor SLAM	

Natural or semi-natural environments. Representative datasets such as UZH-FPV [Delmerico et al. \(2019\)](#), MARS-LVIG [Li et al. \(2024\)](#), and FIREStereo [Dhrafani et al. \(2025\)](#) focus on natural terrains including islands, valleys, grasslands, and forests. These environments introduce challenges such as drastic illumination changes, motion blur, foliage occlusion, texture sparsity, and complex, unstructured geometries, making them valuable for stress-testing perception and navigation systems in outdoor and partially unstructured scenes.

Although the aforementioned datasets have greatly advanced the development of multi-modal SLAM, they predominantly feature environments with clear man-made structures or natural geometric cues, offering stable feature points and semantic anchors for reliable perception and mapping. In contrast, agricultural scenes present fundamentally different and highly degraded conditions: dense and repetitive vegetation, weak textures, frequent occlusion and foliage motion, strong illumination and wind variations, and a lack of stable structural anchors. As a result, current datasets provide limited support for evaluating low-altitude UAV localization and mapping in real precision-agriculture environments.

2.2 Agricultural Datasets

Agricultural datasets have historically emerged from the needs of crop growth monitoring and precision farming, where the primary objectives include plant phenotyping, vegetation segmentation, disease detection, and field-level condition assessment. Only in recent years has the community begun to introduce datasets specifically designed for agricultural SLAM and autonomous navigation. Compared with generic robotics datasets, agricultural datasets are uniquely shaped by crop structure, seasonal variations, and operational constraints, leading to diverse sensing setups and scene characteristics. Existing agricultural datasets can be grouped into four major categories according to platform type, scene structure, and intended task.

Phenotyping and crop-monitoring datasets. Early agricultural datasets, such as Sugar Beets [Chebrolu et al. \(2017\)](#), focus on multi-spectral, RGB-D, and LiDAR measurements for crop classification, inter-row localization, and biomass estimation. These datasets provide rich multimodal signals for static analysis and plant-level tasks, but they are not designed for evaluating UAV-based SLAM pipelines.

Ground robotic SLAM datasets in open farmland. Datasets including Rosario [Pire et al. \(2019\)](#), UnderCanopy [Cuaran et al. \(2024\)](#), and GREENBOT [Cañadas-Aránega et al. \(2024\)](#) capture near-ground navigation in soybean fields, corn rows, and greenhouses using stereo cameras, wheel odometry, IMU, LiDAR, and GNSS. These datasets rely heavily on structured row geometry and near-field texture cues, enabling reliable perception under constrained viewpoints but offering limited diversity in crop types and environmental conditions.

Ground datasets in orchards and plantations. Datasets such as Macadamia Orchard [Islam et al. \(2023\)](#), Citrus-Farm [Teng et al. \(2023\)](#), and MOLO-SLAM [Lv et al. \(2024\)](#) are collected in orchards and vineyards, where trees or vines

form clear vertical structures and repeated spatial patterns. These environments introduce moderate natural variability while still providing stable geometric anchors (tree trunks, trellis systems), which simplify localization compared with open-field row crops.

Limited UAV-based agricultural datasets. A small number of agricultural UAV datasets, such as GrapeSLAM [Wang et al. \(2025a\)](#), explore aerial views over vineyards but remain limited in crop type, spatial scale, and overall scene diversity. The WeedsGalore dataset [Celikkan et al. \(2025\)](#) broadens sensing with multispectral and multi-temporal imagery, yet the absence of LiDAR, full 6-DoF ground truth, and richer geometric structure still restricts its suitability for benchmarking SLAM or reconstruction algorithms in more demanding agricultural settings.

Despite their contributions, the aforementioned datasets predominantly focus on ground platforms, constrained viewpoints, and structured or semi-structured agricultural environments. Most datasets involve a single crop species, a single season, or a limited geographic region, with few providing long-term, multi-season, or multi-terrain coverage. Furthermore, existing UAV-based agricultural datasets remain scarce and are mostly collected in orchards, where stable vertical structures simplify perception. As a result, they fall short of capturing the dense foliage, highly repetitive textures, foliage-induced motion, strong illumination fluctuations, and other degraded conditions commonly encountered by UAVs operating at low altitude over open-field crops.

3 System Overview

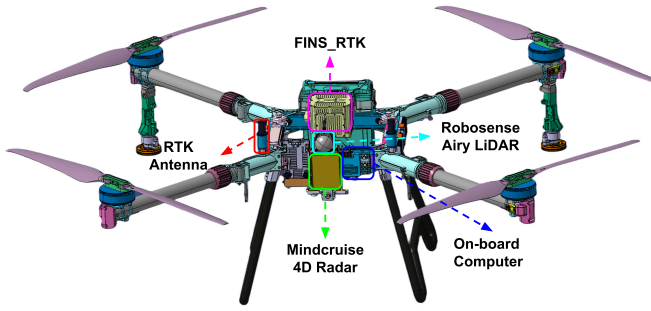
3.1 Sensor Setup

A TopXGun FP300E agricultural UAV* carries a customized SLAM payload consisting of a 3D LiDAR (with an integrated IMU) and a 4D Radar. The platform is equipped with a FINS_RTK navigation module, providing centimeter-level position accuracy and high-fidelity orientation ground truth. All sensor data are logged by an on-board ARM computer based on the RK3588 processor and running the Robot Operating System (ROS). The sensors interface with the computer over Gigabit Ethernet and are synchronized using the IEEE 1588 Precision Time Protocol (PTP). The overall hardware configuration is shown in Figure 1a, and the specifications of each sensor are summarized below.

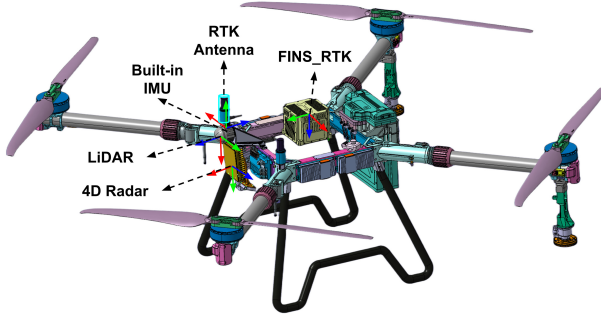
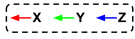
1. **3D LiDAR.** We employ the RoboSense Airy† as a lightweight and cost-effective 3D LiDAR. As shown in Figure 2, it provides a 96-beam configuration with a $90^\circ \times 360^\circ$ FoV and a maximum range of 60 m (or 30 m at 10 % reflectivity in outdoor conditions). The sensor operates at 10 Hz and outputs point clouds with timestamps, ring indices, and reflectivity values. Its large vertical FoV is a key reason for selection, as narrower-coverage alternatives such as Velodyne VLP-16 (30°) or Livox Mid-360 (59°) may fail to

*<https://www.topxgun.com/topxgun-fp300e-agricultural-drone>

†<https://www.robosense.ai/IncrementalComponents/Airy>



(a) Sensor setup on the TopXGun FP300E platform.



(b) Relative positions and coordinate frames of all sensors.

Figure 1. Sensor configuration on the TopXGun FP300E. The onboard setup integrates a RoboSense Airy LiDAR, a Mindcruise 4D Radar, and a FINS_RTK module for ground-truth reference (top), with the relative sensor positions and coordinate frames illustrated below (bottom).

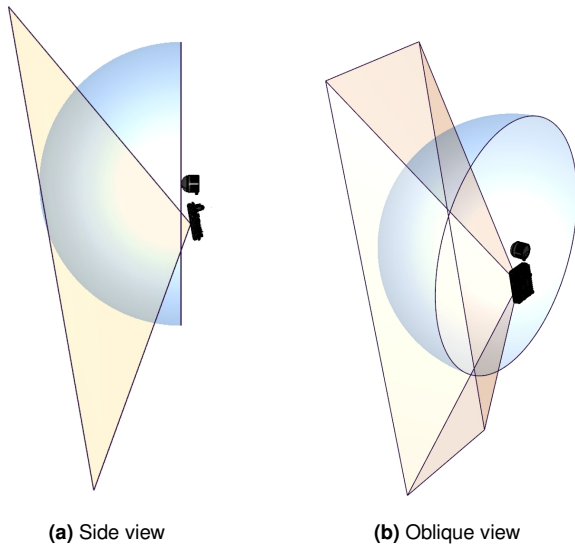


Figure 2. Visualization of the FoV configuration for the LiDAR and 4D Radar. The two viewpoints illustrate their respective sensing coverages, with the LiDAR rendered in blue and the 4D Radar in yellow.

capture sufficient structure in cluttered agricultural environments.

2. **IMU.** The LiDAR integrates an IIM-42652 IMU[‡], providing angular velocity and linear acceleration at 200 Hz. The gyroscope exhibits a bias instability below 3.6 °/h and a Temperature Coefficient of Offset

(TCO) under 0.02 dps/K. The accelerometer offers a TCO of 0.15 mg/K and low spectral noise of $70 \mu\text{g}/\sqrt{\text{Hz}}$. IMU measurements are transmitted via the same Ethernet interface as the LiDAR and logged synchronously in ROS.

3. **4D Radar.** The Mindcruise A1 4D Radar is mounted directly beneath the LiDAR to maximize FoV overlap and improve cross-sensor observability, as shown in Figure 1a and 2. It offers a $60^\circ \times 120^\circ$ FoV and a detection range of up to 100 m. In addition to range and angle, the sensor provides Doppler velocity measurements from -35 m/s to 20 m/s , enabling the direct observation of dynamic targets. Operating at 10 Hz, the Radar delivers reliable performance in dusty or foggy environments due to the longer wavelength of millimeter-wave signals, complementing the LiDAR in challenging agricultural scenarios.
4. **FINS_RTK.** High-precision ground-truth poses are provided by the TJ-FINS70D FINS_RTK module, which fuses FINS inertial measurements with a built-in RTK receiver. The system achieves position accuracy better than $2 \text{ cm} + 1 \text{ ppm}$ (50% CEP), and orientation accuracy of 0.01° (1σ) in roll/pitch and 0.05° (1σ) in yaw. Operating at 100 Hz, this module supplies a reliable reference for quantitative evaluation of SLAM and odometry performance.

3.2 Sensor Calibration

The extrinsic parameters among the LiDAR, the 4D Radar, the RTK antenna phase centers, and the FINS_RTK module are derived directly from the UAV's CAD design files and released together with the dataset (see Figure 1b). Because the internal IMU is rigidly integrated within the LiDAR unit, its relative transform is factory-calibrated and remains constant during data collection.

Accurate LiDAR–Radar extrinsic calibration is crucial for multi-sensor fusion and consistent cross-modal point cloud alignment. We formulate this calibration as a 3D–3D registration problem, aligning the coordinate frames of both sensors within a unified reference. The CAD-derived translation and rotation serve as initial priors, which are subsequently refined through a manual calibration procedure Yan et al. (2022) using multiple corner reflectors placed in the environment. This refinement significantly improves alignment precision compared to the raw CAD configuration, providing a reliable geometric basis for downstream multi-sensor SLAM.

Once calibration is completed, LiDAR and 4D Radar point clouds are transformed into the shared coordinate frame. Figure 3 shows the resulting alignment, demonstrating high spatial consistency across modalities. To further verify calibration accuracy, we visualize two representative scenarios—a static ground sequence and a UAV hovering case—displaying only the overlapping regions of the point clouds for clarity.

[‡]<https://invensense.tdk.com/products/smartindustrial/iim-42652/>

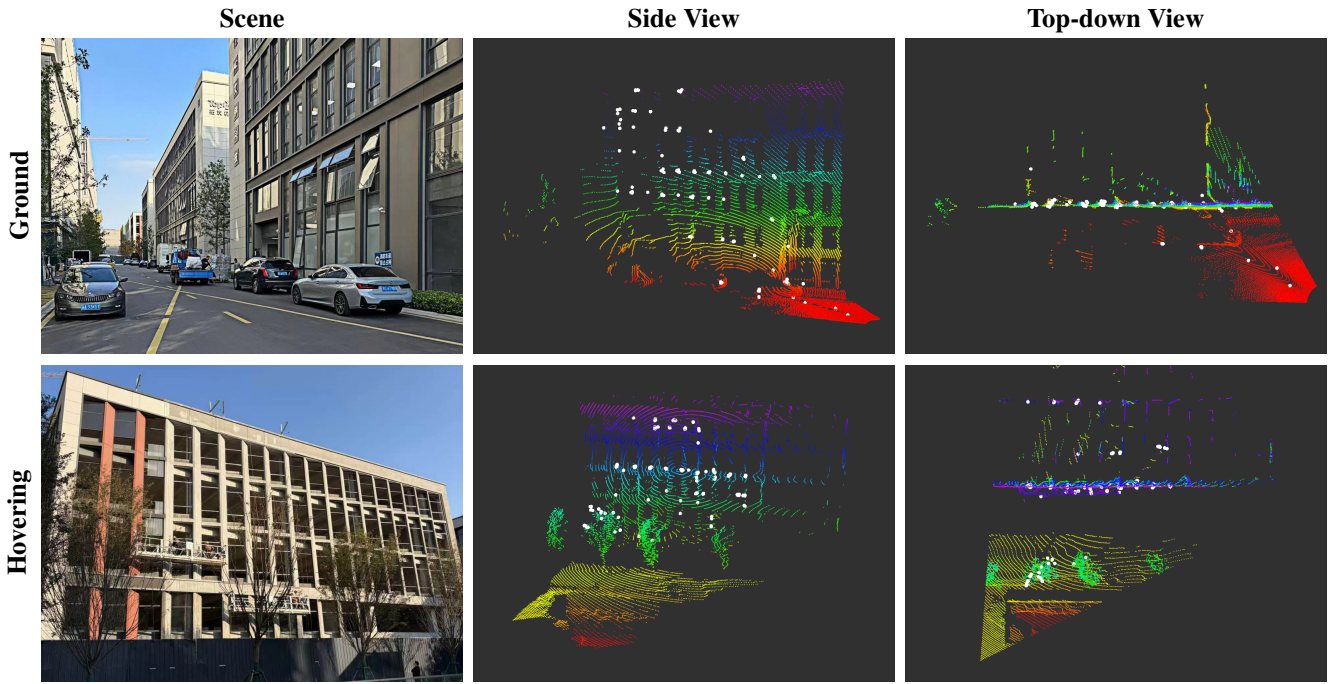


Figure 3. Visualization of the LiDAR and 4D Radar point clouds used to assess the extrinsic calibration. Height-colored LiDAR points and white 4D Radar points are visualized in a common frame following extrinsic alignment, with side and top-down views illustrating the spatial consistency across scenarios.

3.3 Data Format

All sensor data are stored in ROS bag files, a widely adopted standard for synchronized multi-sensor logging and seamless data playback in robotics. The corresponding ROS topics, message types, and update rates are summarized in Table 2.

The LiDAR provides 3D point clouds containing (x, y, z) coordinates with per-point attributes including intensity, ring index, and precise timestamps. The IMU supplies raw inertial measurements consisting of linear acceleration and angular velocity. The 4D Radar generates point clouds enriched with range-angle information, Doppler velocity, Signal-to-Noise Ratio (SNR), and Radar Cross-Section (RCS) values, enabling both geometric and motion-related perception.

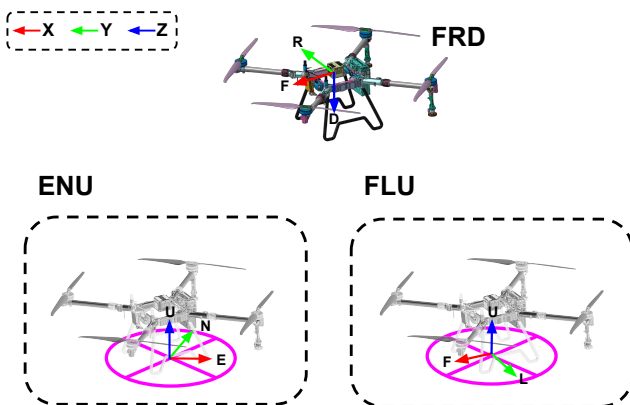


Figure 4. Ground-truth reference frames used in this work. The UAV body frame (FRD) and the two frames relative to the take-off point, FLU and ENU, are shown for defining consistent trajectory coordinates.

To obtain high-precision and easily usable ground-truth trajectories, the FINS-RTK outputs are processed into

three reference forms: (1) a pose reference expressed in the East-North-Up (ENU) frame relative to the take-off location; (2) a pose reference expressed in the Forward-Left-Up (FLU) body frame, also anchored at the take-off point; and (3) a geodetic reference containing latitude, longitude, and altitude in the global coordinate system.

Orientation measurements follow the Front-Right-Down (FRD) aerospace convention. The relationships among these coordinate frames are visualized in Figure 4. These unified ground-truth representations provide a consistent and accurate spatial foundation for benchmarking multi-sensor SLAM algorithms.

4 Dataset Characteristics

To ensure broad scenario diversity, data were collected across three representative farmland terrains—flat plains, hilly regions, and mountainous terraces—located in Nanjing, China. The dataset is organized into six sequence groups based on terrain type and scanning mode (boundary or coverage), namely NJFlatB, NJFlatC, NJHillB, NJHillC, NJTerrB, and NJTerrC.

For all sequences except NJTerrB and NJTerrC, the UAV flew at a constant altitude with respect to the take-off point. In contrast, for the mountainous-terrain sequences NJTerrB and NJTerrC, the UAV maintained a fixed height Above Ground Level (AGL) to ensure flight safety and stable sensor coverage over rapidly varying elevation. Multiple combinations of flight altitudes and speeds were employed to introduce different levels of SLAM difficulty. Each sequence additionally begins with a short stationary or hovering segment to facilitate IMU initialization.

Table 3 summarizes the detailed flight configurations and ROS bags for all sequences. The real-world operational

Table 2. Overview of the sensors employed in the dataset. Each sensor is presented with its associated ROS topics and key specifications, providing a comprehensive reference for data acquisition and integration.

Sensor	Module	Topic Name	Message Type	Rate (Hz)
LiDAR	Robosense Airy	/rslidar_points	sensor_msgs/PointCloud2	10
IMU	Built-in (LiDAR)	/rslidar_imu_data	sensor_msgs/Imu	200
4D Radar	Mindcruise A1	/radar_points	sensor_msgs/PointCloud2	10
FINS_RTK	TJ-FINS70D	/aircraft_pose_enu	geometry_msgs/PoseStamped	100
		/aircraft_pose_flu	geometry_msgs/PoseStamped	100
		/aircraft_position_llh	sensor_msgs/NavSatFix	100

Table 3. Detailed configurations of flight paths and ROS bags for all sequences. The ROS bags are organized into six sequence groups according to terrain category and scanning mode.

Scene	Sequence	Scanning Mode	Altitude (m)	Speed (m/s)	Path Length (m)
Flat farmland	NJFlatB01	boundary	5	3	434.77
	NJFlatB02	boundary	5	8	464.21
	NJFlatB03	boundary	10	3	456.32
	NJFlatB04	boundary	10	8	462.18
	NJFlatB05	boundary	15	3	465.89
	NJFlatB06	boundary	15	8	454.21
	NJFlatC01	coverage	5	8	805.65
	NJFlatC02	coverage	10	3	801.17
	NJFlatC03	coverage	10	8	798.96
	NJFlatC04	coverage	15	3	822.23
Hilly farmland	NJHillB01	boundary	8	3	490.61
	NJHillB02	boundary	8	8	493.07
	NJHillB03	boundary	13	3	480.98
	NJHillB04	boundary	13	8	484.60
	NJHillB05	boundary	18	3	483.84
	NJHillB06	boundary	18	8	488.41
	NJHillC01	coverage	8	3	776.47
	NJHillC02	coverage	8	8	783.31
	NJHillC03	coverage	13	3	761.55
	NJHillC04	coverage	13	8	768.14
	NJHillC05	coverage	18	3	756.07
	NJHillC06	coverage	18	8	769.94
Terraced farmland	NJTerrB01	boundary	3	3	204.91
	NJTerrB02	boundary	6	3	207.21
	NJTerrB03	boundary	6	6	209.71
	NJTerrB04	boundary	9	3	211.95
	NJTerrB05	boundary	9	6	215.72
	NJTerrC01	coverage	3	3	311.23
	NJTerrC02	coverage	3	6	307.53
	NJTerrC03	coverage	6	3	311.24
	NJTerrC04	coverage	6	6	300.84
	NJTerrC05	coverage	9	3	313.64
	NJTerrC06	coverage	9	6	317.48

configurations, along with the corresponding UAV waypoint layouts, are illustrated in Figure 5.

4.1 Flat Farmland

The NJFlatB and NJFlatC sequences were collected in flat agricultural fields consisting of nearly mature sorghum awaiting harvest (31.8921°N, 118.8548°E). As illustrated in Figure 5, the area spans approximately 250 m by 350 m, bordered in part by sparse trees and utility poles. The

uniformly grown sorghum and largely featureless terrain yield minimal geometric variation, creating a challenging setting for feature extraction, data association, and stable state estimation. Two scanning modes were used, with flight altitudes relative to the take-off point at 5 m, 10 m, and 15 m, and speeds of 3 m/s or 8 m/s, providing sequences with different motion dynamics and viewpoints.

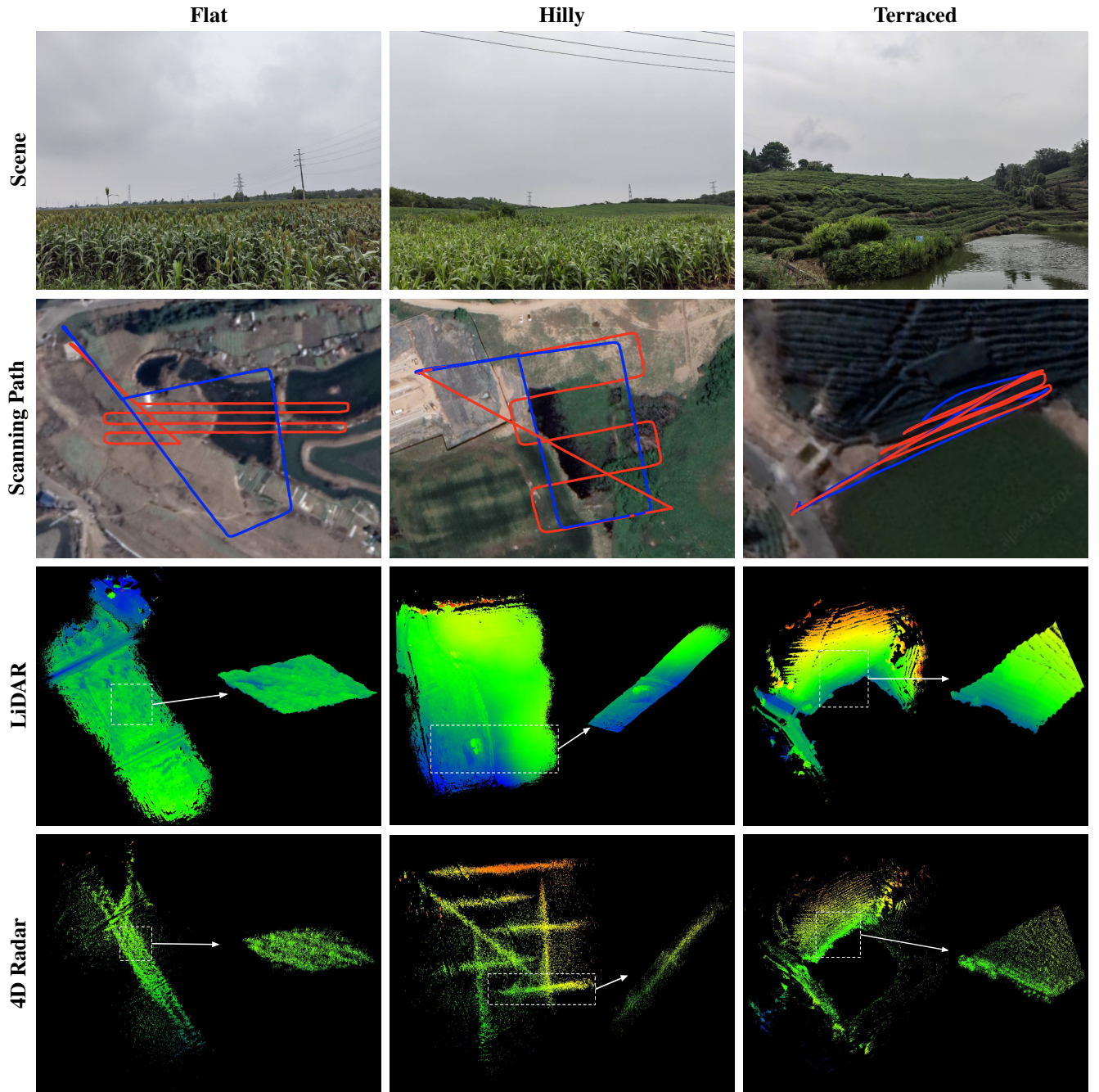


Figure 5. Visualization of the three representative farmland scenarios and their corresponding sensor data. Each column corresponds to a distinct terrain type: flat farmland, hilly farmland, and terraced farmland. From top to bottom, subfigures illustrate the real-world operation scenes, boundary (blue) and coverage (red) scanning paths, and the top-view height-colored LiDAR (Faster-LIO [Bai et al. \(2022\)](#)) and 4D Radar (GaRLIO [Noh et al. \(2025\)](#)) maps, with zoomed-in regions highlighting local geometric details.

4.2 Hilly Farmland

The NJHillB and NJHillC sequences were captured over gently sloped farmland in hilly terrain (31.8348°N, 118.7813°E). The 180 m by 280 m area features moderate slopes of approximately 15°, with lower regions planted with mature sorghum and upper regions covered by short grass. A dense tree line forms one boundary of the site (see Figure 5). The mixture of vegetation types and sloped geometry results in more structural cues than flat farmland, though still with limited distinctive features, offering a moderately challenging SLAM environment. Data were recorded in two

scanning modes at constant heights from the take-off point (8 m, 13 m, 18 m) and at flight speeds of 3 m/s and 8 m/s.

4.3 Terraced Farmland

The NJTerrB and NJTerrC sequences were acquired in steep mountainous terrain consisting of terraced farmland primarily used for tea cultivation (31.7737°N, 118.6917°E). The area covers roughly 100 m by 100 m, with slopes around 45°. Tea plants are grown along consistent contour lines, forming distinctive terrace patterns rich in geometric cues, as shown in Figure 5. The combination of pronounced elevation changes and structured tea canopies makes this environment

relatively favorable for SLAM. For safe operation in the steep terrain, the UAV took off from a road at the base of the terraces and maintained a constant height Above Ground Level (3 m, 6 m, 9 m) while flying at 3 m/s or 6 m/s.

5 Experiments

5.1 Benchmark Methods and Evaluation

To thoroughly assess the proposed AgriLiRa4D dataset, we benchmark representative state-of-the-art multi-sensor SLAM algorithms covering three major sensing modalities: LiDAR–Inertial Odometry (LIO), Radar–Inertial Odometry (RIO), and Radar–LiDAR–Inertial Odometry (RLIO). LIO approaches such as FAST-LIO2 [Xu et al. \(2022\)](#), Faster-LIO [Bai et al. \(2022\)](#), LIO-SAM [Shan et al. \(2020a\)](#), and LiLi-OM [Li et al. \(2021\)](#) fuse dense LiDAR scans with IMU integration and are widely adopted for precise odometry in structured and semi-structured environments. RIO methods, including EKF-RIO [Doer and Trommer \(2020\)](#), DRIO [Chen et al. \(2023\)](#), and 4D-IRIOM [Zhuang et al. \(2023\)](#), leverage Radar’s robustness against visual and geometric degradation, while Doppler measurements provide additional motion cues when LiDAR becomes unreliable. RLIO frameworks such as DR-LRIO [Nissov et al. \(2024\)](#), AF-RLIO [Qian et al. \(2025\)](#), and GaRLIO [Noh et al. \(2025\)](#) further integrate the complementary characteristics of all three modalities to achieve enhanced consistency and robustness under challenging conditions.

Considering practical constraints such as open-source availability, implementation stability, and compatibility with our GNSS-free and vision-free evaluation protocol, we selected four algorithms for benchmarking: FAST-LIO2 and Faster-LIO for LIO, EKF-RIO for RIO, and GaRLIO for RLIO. Other representative methods discussed above were not included because many lack official open-source implementations, rely on sensing modalities that are not available in our dataset (such as visual, depth, or GNSS measurements), or require hardware interfaces and engineering adaptations that hinder reproducible large-scale evaluation. Overall, the selected four algorithms provide representative and reliable baselines that cover the LIO, RIO, and RLIO modality spectrum for benchmarking on AgriLiRa4D.

Performance is evaluated using the Root Mean Square Error (RMSE) of the Absolute Trajectory Error (ATE), computed after aligning each estimated trajectory with the high-precision FINS-RTK ground truth. All evaluations are performed using the evo toolkit [Grupp \(2017\)](#) to ensure consistency and reproducibility, with translational and rotational errors reported in meters and degrees, respectively. The quantitative results across different farmland scenarios and flight configurations are summarized in Table 4, providing a comprehensive comparison of the selected algorithms under varied environmental and operational conditions. A run is considered a failure if the translational ATE relative to the path length (Table 3) exceeds 15%, or if the rotational ATE exceeds 45° .

5.2 Overall Benchmark Performance

Across all evaluated sequences, the LIO methods deliver the most stable and consistently accurate performance on the AgriLiRa4D dataset. Both FAST-LIO2 and Faster-LIO achieve the lowest ATE in the majority of sequences and maintain reliable operation across all farmland types, with only moderate degradation under higher altitudes or faster flight speeds. In contrast, the RIO baseline, EKF-RIO, exhibits the least stable behavior, failing on nearly all flat farmland sequences and showing large drift even in those hilly and terraced sequences where it successfully completes a run. The RLIO method GaRLIO demonstrates mixed performance: it frequently fails in hilly farmland, operates inconsistently in flat terrain, but achieves its most stable and competitive results in terraced farmland, where it occasionally matches or slightly outperforms the LIO baselines in rotation accuracy. Overall, the benchmark outcomes highlight a wide difficulty spectrum across sensing modalities and farmland types, demonstrating that AgriLiRa4D offers a comprehensive and discriminative testbed for evaluating multi-sensor SLAM robustness in real agricultural environments.

5.3 Impact of Sensing Modality

The performance differences observed among LIO, RIO, and RLIO methods can be largely attributed to the sensing characteristics and the original design intentions of each modality. LIO approaches, represented by FAST-LIO2 and Faster-LIO, inherently benefit from dense geometric constraints and tight LiDAR–IMU coupling. Both methods were originally validated on UAV platforms—including indoor and outdoor flight scenarios—making them naturally suited for the fast motion, wide-area scanning, and geometry-rich conditions typical of agricultural UAV operation. This strong geometric anchoring explains why LIO methods remain the most stable across all terrain types in our dataset.

In contrast, the RIO baseline EKF-RIO shows limited robustness in outdoor agricultural environments. Although EKF-RIO was originally evaluated on UAVs, its validation was restricted to indoor settings, where Radar returns are much denser and more structured. In large open agricultural fields, 4D Radar often produces sparse and noisy returns, especially over flat crops or grass surfaces, resulting in insufficient geometric constraints for stable odometry. Moreover, Radar measurements are highly sensitive to dynamic vegetation induced by UAV downwash, producing fluctuating point responses that challenge consistent data association. While Doppler velocity provides valuable motion cues, these cues become unreliable when the underlying spatial structure is weak, contributing to the significant drift and frequent failures observed in our evaluation.

The RLIO method GaRLIO exhibits mixed performance due to its sensing design and domain mismatch. GaRLIO was originally developed and tested primarily on Unmanned Ground Vehicle (UGV) platforms with near-ground viewpoints, balanced LiDAR–Radar overlap, and slower, more stable motion profiles. When applied to UAV flights, several mismatches arise: LiDAR–Radar common visibility decreases with altitude, Doppler signatures change

Table 4. Translation (meters) and rotation (degrees) RMSE of the ATE for the evaluated methods on the AgriLiRa4D dataset. For each sequence, results are **bold** for best, and underlined for second best. A dash (“-”) signifies the failure of the algorithm’s execution.

Scene	Sequence	FAST-LIO2		Faster-LIO		EKF-RIO		GaRLIO	
		ATE _r	ATE _t	ATE _r	ATE _t	ATE _r	ATE _t	ATE _r	ATE _t
Flat farmland	NJFlatB01	6.67	9.38	4.33	3.73	-	-	<u>4.46</u>	<u>4.08</u>
	NJFlatB02	<u>5.68</u>	4.60	6.12	<u>3.19</u>	-	-	4.35	2.75
	NJFlatB03	<u>4.06</u>	<u>5.68</u>	3.20	3.76	-	-	4.87	7.21
	NJFlatB04	3.55	<u>3.73</u>	3.79	4.44	19.51	29.47	<u>3.68</u>	2.91
	NJFlatB05	4.57	7.04	2.83	3.10	-	-	<u>3.02</u>	<u>6.07</u>
	NJFlatB06	<u>7.64</u>	<u>8.69</u>	4.91	4.74	-	-	19.82	44.65
	NJFlatC01	20.48	40.60	6.12	8.37	<u>15.93</u>	<u>31.56</u>	16.80	64.36
	NJFlatC02	7.15	15.05	3.05	4.33	16.72	82.66	<u>5.03</u>	<u>7.72</u>
	NJFlatC03	4.92	7.42	3.08	<u>4.54</u>	22.67	40.39	<u>3.18</u>	4.16
	NJFlatC04	<u>3.61</u>	<u>5.57</u>	2.80	2.58	-	-	-	-
	NJHillB01	<u>5.16</u>	<u>8.05</u>	3.96	4.55	6.70	11.64	-	-
	NJHillB02	<u>4.48</u>	<u>4.50</u>	3.78	3.54	43.27	53.06	-	-
Hilly farmland	NJHillB03	<u>5.52</u>	<u>6.48</u>	4.48	4.24	15.77	20.33	-	-
	NJHillB04	<u>6.58</u>	<u>7.85</u>	3.73	4.28	43.59	56.02	-	-
	NJHillB05	3.60	46.15	6.08	63.22	20.60	<u>28.18</u>	<u>4.43</u>	5.84
	NJHillB06	<u>5.30</u>	<u>3.80</u>	2.79	3.10	14.14	28.64	7.01	25.05
	NJHillC01	<u>15.37</u>	<u>47.85</u>	6.46	12.06	-	-	-	-
	NJHillC02	<u>8.71</u>	<u>18.97</u>	-	-	-	-	7.94	11.69
	NJHillC03	6.57	41.13	<u>6.44</u>	<u>20.46</u>	-	-	5.07	10.12
	NJHillC04	7.22	24.60	3.62	<u>5.15</u>	9.62	23.18	<u>4.22</u>	4.36
	NJHillC05	4.52	26.57	-	-	-	-	-	-
	NJHillC06	<u>6.29</u>	20.08	3.63	<u>26.15</u>	42.98	64.17	-	-
	NJTerrB01	2.67	<u>0.70</u>	<u>2.69</u>	0.67	5.42	5.03	3.06	1.67
Terraced farmland	NJTerrB02	2.61	0.51	<u>2.64</u>	<u>0.61</u>	17.59	9.33	21.54	15.41
	NJTerrB03	2.22	<u>0.51</u>	<u>2.55</u>	0.50	32.92	15.91	21.18	17.62
	NJTerrB04	2.63	<u>0.74</u>	<u>2.77</u>	0.73	3.43	4.03	38.13	17.82
	NJTerrB05	<u>6.60</u>	<u>3.60</u>	3.70	1.50	-	-	20.56	14.50
	NJTerrC01	3.02	<u>0.93</u>	<u>3.07</u>	0.92	-	-	8.35	5.12
	NJTerrC02	<u>4.39</u>	<u>2.27</u>	2.79	0.76	21.93	13.49	12.98	7.66
	NJTerrC03	2.63	1.14	<u>3.56</u>	<u>2.47</u>	12.20	7.24	7.16	11.54
	NJTerrC04	<u>2.67</u>	1.21	2.66	<u>1.66</u>	-	-	8.14	10.46
	NJTerrC05	2.32	<u>1.02</u>	2.22	0.62	6.14	6.72	<u>2.27</u>	1.05
	NJTerrC06	2.70	1.89	25.21	21.58	-	-	<u>4.05</u>	<u>2.82</u>

under fast aerial motion, and Radar becomes more sensitive to vegetation-driven perturbations. Consequently, GaRLIO occasionally outperforms LIO in hilly farmland as shown in Figure 6 and Figure 7, where the sloped terrain provides stronger and more distinguishable Radar returns that compensate for its reduced LiDAR support.

Across all modalities, a common trend is that positional drift predominantly accumulates along the vertical (Z) axis, as illustrated in Figure 7 for the NJHillC04 sequence. This behavior is consistent with the sensing geometry: airborne LiDAR primarily observes the environment from near-horizontal viewpoints, providing weaker constraints on altitude compared to horizontal motion, while 4D Radar exhibits coarser elevation resolution. As a result, Z-axis estimation relies more heavily on IMU integration, making it particularly susceptible to drift when geometric structure or Radar elevation cues are insufficient.

5.4 Effect of Terrain, Vegetation and Altitude

The varying performance across different farmland types in AgriLiRa4D can be explained by the combined effects of terrain geometry, vegetation characteristics, and flight parameters such as altitude and speed. As shown in Figure 5, terraced farmland consistently yields the most favorable results for all methods due to its strong and repetitive geometric contours. The steep slopes and layered tea canopies create stable depth gradients that offer abundant geometric constraints for LiDAR-based matching and informative Doppler patterns for Radar processing. These structural advantages allow even the weaker sensing modalities, such as RIO, to complete trajectories reliably and also lead to GaRLIO’s best overall performance in this terrain category.

In contrast, flat farmland represents the most challenging scenario in the dataset. The nearly uniform sorghum fields provide minimal 3D geometric variation, resulting in

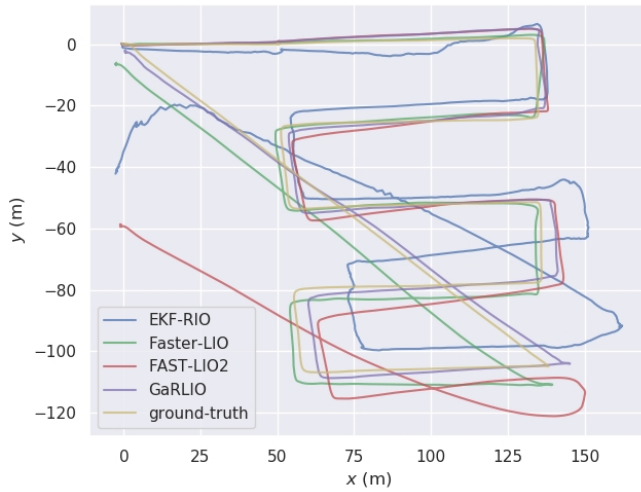


Figure 6. Top-down view comparison of trajectories for the NJHi11C04 sequence. The FINS.RTK ground truth trajectory is presented as the benchmark reference, together with four algorithm-estimated trajectories for performance comparison.

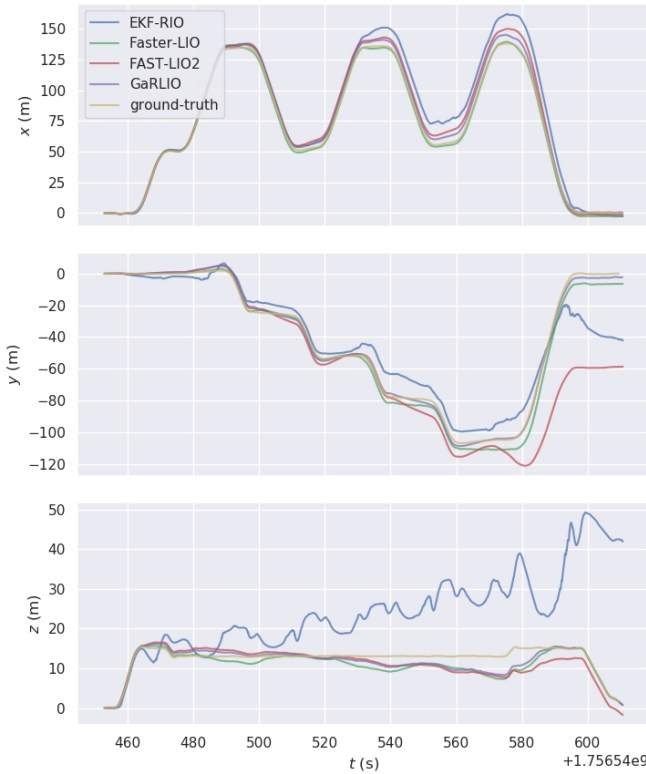


Figure 7. Position errors for the NJHi11C04 sequence. The errors of four algorithms relative to the FINS.RTK ground truth are decomposed and displayed along the X, Y, and Z axes, respectively.

sparse LiDAR features and weak Radar returns, illustrated in Figure 5. The highly repetitive crop-row patterns further complicate data association, magnifying drift for all SLAM systems. Dynamic vegetation motion induced by UAV down-wash contributes additional instability: sorghum stalks sway noticeably at the evaluated flight speeds of 3 m/s and 8 m/s, generating fluctuating LiDAR edges and volatile Radar reflections. These factors collectively explain the significant

performance degradation observed in flat farmland, particularly in the high-speed (NJFlatB02/B04/B06) and long-path coverage sequences (NJFlatC01-C04), where the longest trajectories exceed 800 m.

Hilly farmland presents intermediate difficulty. Although the terrain contains noticeable elevation changes, the local surface patches observed from typical UAV altitudes remain nearly planar for LiDAR, offering limited improvement for LIO compared with flat fields. In contrast, Radar is more sensitive to terrain gradients, primarily due to its substantially longer sensing range. This extended visibility enables RLIO to occasionally benefit from the sloped ground geometry. At the same time, grassy and shrub-covered surfaces in hilly regions remain vulnerable to wind-induced motion, introducing fluctuations in both LiDAR and Radar measurements.

Flight altitude further modulates the effective sensing quality across all scenes. As altitude increases from 3 m to 18 m (see Table 3), LiDAR beams intersect the ground at progressively shallower angles, reducing point density and diminishing geometric distinctiveness. Radar detections also become sparser and less reliable at higher elevations. These altitude-induced limitations also reduce the spatial overlap between LiDAR and Radar, weakening the cross-modal constraints required by RLIO systems. As a result, sequences flown at higher altitudes—such as NJFlatC04 and NJHi11C05—exhibit higher failure rates and larger trajectory errors across all modalities.

6 Conclusion and Future Work

In this paper, we presented AgriLiRa4D, a multi-modal UAV dataset specifically designed to address the challenges of SLAM and localization in real agricultural environments. The dataset covers three representative farmland types and two flight modes, delivering diverse motion patterns and sensing conditions that are rarely included in existing benchmarks. AgriLiRa4D offers high-precision FINS.RTK ground truth, time-synchronized LiDAR, 4D Radar, and IMU measurements, as well as full calibration data, providing a reliable foundation for developing and evaluating multi-sensor fusion algorithms. Using this dataset, we benchmarked several state-of-the-art multi-sensor SLAM algorithms and highlighted the intrinsic difficulties posed by low-texture crops, repetitive planting structures, uneven terrain, and vegetation dynamics. These results underscore both the difficulty of the sequences and the importance of multi-modal fusion for achieving robust localization in agricultural settings.

Looking ahead, we plan to extend AgriLiRa4D with additional crop types, seasonal variations, and more extreme operational conditions, such as night flights and adverse weather, to further support research on resilient agricultural autonomy. We believe AgriLiRa4D will serve as a long-term resource for the robotics community, catalyzing progress in robust perception and navigation for agricultural UAVs. The challenges surfaced through this benchmark will guide our future work toward developing more resilient, adaptive, and generalizable SLAM frameworks capable of handling the complex, dynamic, and often ambiguous conditions intrinsic to real-world agricultural environments.

Acknowledgements

The authors would like to take this opportunity to thank RoboSense (Suteng Innovation Technology Co., Ltd.) for providing the Airy sensor, which was used to collect some of the data for our experiment and to conduct validations.

References

- Bai C, Xiao T, Chen Y, Wang H, Zhang F and Gao X (2022) Faster-lío: Lightweight tightly coupled lidar-inertial odometry using parallel sparse incremental voxels. *IEEE Robotics and Automation Letters* 7(2): 4861–4868. DOI:10.1109/LRA.2022.3152830.
- Burri M, Nikolic J, Gohl P, Schneider T, Rehder J, Omari S, Achtelik MW and Siegwart R (2016) The euroc micro aerial vehicle datasets. *The International Journal of Robotics Research* 35(10): 1157–1163. DOI:10.1177/0278364915620033. URL <https://doi.org/10.1177/0278364915620033>.
- Cadena C, Carlone L, Carrillo H, Latif Y, Scaramuzza D, Neira J, Reid I and Leonard JJ (2017) Past, present, and future of simultaneous localization and mapping: Toward the robust-perception age. *IEEE Transactions on robotics* 32(6): 1309–1332.
- Cañadas-Aránega F, Blanco-Claraco JL, Moreno JC and Rodríguez-Díaz F (2024) Multimodal mobile robotic dataset for a typical mediterranean greenhouse: The greenbot dataset. *Sensors* 24(6). DOI:10.3390/s24061874. URL <https://www.mdpi.com/1424-8220/24/6/1874>.
- Celikkan E, Kunzmann T, Yeskalyev Y, Itzerott S, Klein N and Herold M (2025) WeedsGalore: A Multispectral and Multitemporal UAV-Based Dataset for Crop and Weed Segmentation in Agricultural Maize Fields. In: *2025 IEEE/CVF Winter Conference on Applications of Computer Vision (WACV)*. Los Alamitos, CA, USA: IEEE Computer Society, pp. 4767–4777. DOI:10.1109/WACV61041.2025.00467. URL <https://doi.ieeecomputersociety.org/10.1109/WACV61041.2025.00467>.
- Chebrolu N, Lottes P, Schaefer A, Winterhalter W, Burgard W and Stachniss C (2017) Agricultural robot dataset for plant classification, localization and mapping on sugar beet fields. *The International Journal of Robotics Research* 36(10): 1045–1052. DOI:10.1177/0278364917720510. URL <https://doi.org/10.1177/0278364917720510>.
- Chen H, Liu Y and Cheng Y (2023) Drio: Robust radar-inertial odometry in dynamic environments. *IEEE Robotics and Automation Letters* 8(9): 5918–5925. DOI:10.1109/LRA.2023.3301290.
- Cheng D, Yao Y, Liu R, Li X, Guan B and Yu F (2023) Precision agriculture management based on a surrogate model assisted multiobjective algorithmic framework. *Scientific Reports* 13(1): 1142.
- Cuaran J, Velasquez AEB, Gasparino MV, Uppalapati NK, Sivakumar AN, Wasserman J, Huzaifa M, Adve S and Chowdhary G (2024) Under-canopy dataset for advancing simultaneous localization and mapping in agricultural robotics. *The International Journal of Robotics Research* 43(6): 739–749. DOI:10.1177/02783649231215372. URL <https://doi.org/10.1177/02783649231215372>.
- Delmerico J, Cieslewski T, Rebecq H, Faessler M and Scaramuzza D (2019) Are we ready for autonomous drone racing? the uzh-fpv drone racing dataset. In: *2019 International Conference on Robotics and Automation (ICRA)*. pp. 6713–6719. DOI: 10.1109/ICRA.2019.8793887.
- Dhrafani D, Liu Y, Jong A, Shin U, He Y, Harp T, Hu Y, Oh J and Scherer S (2025) Firestereo: Forest infrared stereo dataset for uas depth perception in visually degraded environments. *IEEE Robotics and Automation Letters* 10(4): 3302–3309. DOI: 10.1109/LRA.2025.3536278.
- Doer C and Trommer GF (2020) Radar inertial odometry with online calibration. In: *2020 European Navigation Conference (ENC)*. pp. 1–10. DOI:10.23919/ENC48637.2020.9317343.
- Grupp M (2017) evo: Python package for the evaluation of odometry and slam. <https://github.com/MichaelGrupp/evo>.
- He J, Zhan Z, Tu Z, Zhu X and Yuan J (2025) A multi-sensor fusion approach for rapid orthoimage generation in large-scale uav mapping. In: *2025 IEEE/RSJ International Conference on Intelligent Robots and Systems (IROS)*. pp. 6808–6815. DOI: 10.1109/IROS60139.2025.11247677.
- Islam R, Habibullah H and Hossain T (2023) Agri-slam: a real-time stereo visual slam for agricultural environment. *Autonomous Robots* 47(6): 649–668. DOI:10.1007/s10514-023-10110-y. URL <https://doi.org/10.1007/s10514-023-10110-y>.
- Li H, Zou Y, Chen N, Lin J, Liu X, Xu W, Zheng C, Li R, He D, Kong F, Cai Y, Liu Z, Zhou S, Xue K and Zhang F (2024) Mars-lvig dataset: A multi-sensor aerial robots slam dataset for lidar-visual-inertial-gnss fusion. *The International Journal of Robotics Research* 43(8): 1114–1127. DOI:10.1177/02783649241227968. URL <https://doi.org/10.1177/02783649241227968>.
- Li K, Li M and Hanebeck UD (2021) Towards high-performance solid-state-lidar-inertial odometry and mapping. *IEEE Robotics and Automation Letters* 6(3): 5167–5174. DOI: 10.1109/LRA.2021.3070251.
- Lv J, Yao B, Guo H, Gao C, Wu W, Li J, Sun S and Luo Q (2024) Molo-slam: A semantic slam for accurate removal of dynamic objects in agricultural environments. *Agriculture* 14(6). DOI: 10.3390/agriculture14060819. URL <https://www.mdpi.com/2077-0472/14/6/819>.
- Majdik AL, Till C and Scaramuzza D (2017) The zurich urban micro aerial vehicle dataset. *The International Journal of Robotics Research* 36(3): 269–273. DOI:10.1177/0278364917702237. URL <https://doi.org/10.1177/0278364917702237>.
- Mur-Artal R and Tardós JD (2017) Orb-slam2: An open-source slam system for monocular, stereo, and rgb-d cameras. *IEEE transactions on robotics* 33(5): 1255–1262.
- Nguyen TM, Yuan S, Cao M, Lyu Y, Nguyen TH and Xie L (2022) Ntu viral: A visual-inertial-ranging-lidar dataset, from an aerial vehicle viewpoint. *The International Journal of Robotics Research* 41(3): 270–280. DOI:10.1177/02783649211052312. URL <https://doi.org/10.1177/02783649211052312>.
- Nissov M, Khedekar N and Alexis K (2024) Degradation resilient lidar-radar-inertial odometry. In: *2024 IEEE International Conference on Robotics and Automation (ICRA)*. pp. 8587–8594. DOI:10.1109/ICRA57147.2024.10611444.

- Noh C, Yang W, Jung M, Jung S and Kim A (2025) Garlio: Gravity enhanced radar-lidar-inertial odometry. URL <https://arxiv.org/abs/2502.07703>.
- Pini M, Maruccio G, Falco G, Nicola M and De Wilde W (2020) Experimental testbed and methodology for the assessment of rtk gnss receivers used in precision agriculture. *IEEE access* 8: 14690–14703.
- Pire T, Mujica M, Civera J and Kofman E (2019) The rosario dataset: Multisensor data for localization and mapping in agricultural environments. *The International Journal of Robotics Research* 38(6): 633–641. DOI:10.1177/0278364919841437. URL <https://doi.org/10.1177/0278364919841437>.
- Qian C, Xu Y, Shi X, Chen J and Li L (2025) Af-rlio: Adaptive fusion of radar-lidar-inertial information for robust odometry in challenging environments. In: *2025 IEEE International Conference on Robotics and Automation (ICRA)*. pp. 1–7. DOI: 10.1109/ICRA55743.2025.11128046.
- Radoglou-Grammatikis P, Sarigiannidis P, Lagkas T and Moscholiou I (2020) A compilation of uav applications for precision agriculture. *Computer Networks* 172: 107148.
- Shan T, Englot B, Meyers D, Wang W, Ratti C and Daniela R (2020a) Lio-sam: Tightly-coupled lidar inertial odometry via smoothing and mapping. In: *IEEE/RSJ International Conference on Intelligent Robots and Systems (IROS)*. IEEE, pp. 5135–5142.
- Shan T, Englot B, Meyers D, Wang W, Ratti C and Rus D (2020b) Lio-sam: Tightly-coupled lidar inertial odometry via smoothing and mapping. In: *2020 IEEE/RSJ international conference on intelligent robots and systems (IROS)*. IEEE, pp. 5135–5142.
- Sun K, Mohta K, Pfrommer B, Watterson M, Liu S, Mulgaonkar Y, Taylor CJ and Kumar V (2018) Robust stereo visual inertial odometry for fast autonomous flight. *IEEE Robotics and Automation Letters* 3(2): 965–972. DOI:10.1109/LRA.2018.2793349.
- Teng H, Wang Y, Song X and Karydis K (2023) Multimodal dataset for localization, mapping and crop monitoring in citrus tree farms. In: Bebis G, Ghiasi G, Fang Y, Sharf A, Dong Y, Weaver C, Leo Z, LaViola Jr JJ and Kohli L (eds.) *Advances in Visual Computing*. Cham: Springer Nature Switzerland. ISBN 978-3-031-47969-4, pp. 571–582.
- Wang K, Vélez S, Kooistra L, Wang W and Valente J (2025a) GrapeSLAM: UAV-based monocular visual dataset for SLAM, SfM and 3d reconstruction with trajectories under challenging illumination conditions 60: 111495. DOI:<https://doi.org/10.1016/j.dib.2025.111495>. URL <https://www.sciencedirect.com/science/article/pii/S2352340925002276>.
- Wang Q, Zhan Z, He J, Tu Z, Zhu X and Yuan J (2025b) High-quality spatial reconstruction and orthoimage generation using efficient 2d gaussian splatting. URL <https://arxiv.org/abs/2503.19703>.
- Xu H, Liu P, Chen X and Shen S (2024) d^2 slam: Decentralized and distributed collaborative visual-inertial slam system for aerial swarm. *IEEE Transactions on Robotics* 40: 3445–3464. DOI: 10.1109/TRO.2024.3422003.
- Xu W, Cai Y, He D, Lin J and Zhang F (2022) Fast-lio2: Fast direct lidar-inertial odometry. *IEEE Transactions on Robotics* 38(4): 2053–2073. DOI:10.1109/TRO.2022.3141876.
- Yan G, Liu Z, Wang C, Shi C, Wei P, Cai X, Ma T, Liu Z, Zhong Z, Liu Y, Zhao M, Ma Z and Li Y (2022) Opencalib: A multi-sensor calibration toolbox for autonomous driving. *arXiv preprint arXiv:2205.14087*.
- Zhang J, Zhuge H, Wu Z, Peng G, Wen M, Liu Y and Wang D (2023) 4dradarslam: A 4d imaging radar slam system for large-scale environments based on pose graph optimization. In: *2023 IEEE International Conference on Robotics and Automation (ICRA)*. IEEE, pp. 8333–8340.
- Zheng C, Xu W, Zou Z, Hua T, Yuan C, He D, Zhou B, Liu Z, Lin J, Zhu F, Ren Y, Wang R, Meng F and Zhang F (2025) Fast-lio2: Fast, direct lidar–inertial–visual odometry. *IEEE Transactions on Robotics* 41: 326–346. DOI:10.1109/TRO.2024.3502198.
- Zhu Y, Kong Y, Jie Y, Xu S and Cheng H (2023) Graco: A multimodal dataset for ground and aerial cooperative localization and mapping. *IEEE Robotics and Automation Letters* 8(2): 966–973. DOI:10.1109/LRA.2023.3234802.
- Zhuang Y, Wang B, Huai J and Li M (2023) 4d iriom: 4d imaging radar inertial odometry and mapping. *IEEE Robotics and Automation Letters* 8(6): 3246–3253.
- Zuo X, Geneva P, Lee W, Liu Y and Huang G (2019) Lic-fusion: Lidar-inertial-camera odometry. In: *2019 IEEE/RSJ International Conference on Intelligent Robots and Systems (IROS)*. IEEE, pp. 5848–5854.